

Photocatalytic Eosin Y Disproportionation as Driving Force for Terpene Cyclizations

T. Rittner,^{a,+} C. Lucht,^{b,+} N. Rascón,^c A. Abramov,^d L. Hetzel,^e C. J. Stein,^{e,f} R. Gschwind,^d P. Nuernberger,^{a*} T. Gulder^{b,c,g*}

[a] Institute of Physical and Theoretical Chemistry, Faculty of Chemistry and Pharmacy, University Regensburg, Universitätsstraße 31, 93053 Regensburg, Germany

[b] Department for Organic Chemistry, Leipzig University, Johannisallee 29, 04103 Leipzig, Germany

[c] Organic Chemistry, Saarland University, 66123 Saarbruecken, Germany

[d] Institute of Organic Chemistry, Faculty of Chemistry and Pharmacy, University Regensburg, Universitätsstraße 31, 93053 Regensburg, Germany

[e] Department of Chemistry and Catalysis Research Center, School of Natural Sciences, Technical University of Munich, Lichtenbergstraße 4, D-85747 Garching, Germany

[f] Atomistic Modeling Center, Munich Data Science Institute, Technical University of Munich, 85748 Garching, Germany

[g] Synthesis of Natural-Product Derived Drugs, Helmholtz Institute for Pharmaceutical Research Saarland (HIPS) Helmholtz Centre for Infection Research (HZI), 66123 Saarbruecken, Germany

+Both authors contributed equally

E-mail: tanja.gulder@uni-saarland.de

Abstract: A mechanistic paradigm for terpene cyclization driven by photocatalytic disproportionation of eosin Y in fluorinated alcohol media was discovered. By employing a 1:1 mixture of HFIP and PFTB, the neutral form of eosin Y (EH₂) undergoes efficient intersystem crossing to its triplet state, initiating hydrogen atom transfer (HAT) with ground-state EH₂. This generates two radicals, EH[•] and EH₃[•], with EH[•] identified as the key species triggering polyene cyclizations. Spectroscopic and computational analyses revealed that hydrogen bonding with fluorinated alcohols stabilizes the otherwise unfavored open carboxylic acid form of eosin Y, enabling visible-light absorption and reactivity. The study clarifies the long-debated mechanism of eosin Y-mediated cyclizations, introducing a dual-radical generation strategy from a single photocatalyst molecule. These findings introduce a new paradigm in photoredox catalysis, offering a mild, selective, and sustainable approach to complex terpene synthesis and paving the way for broader applications in synthetic organic chemistry.

Biosynthetic polycyclization cascades elegantly demonstrate how nature efficiently achieves the total synthesis of secondary metabolites. A notable example is polyene cyclization, which generates structurally complex, multi-cyclic carbon frameworks from simple linear isoprenyl chains in a single step.^[1-2] This remarkable process simultaneously forms multiple carbon-carbon bonds and stereocenters. Synthetic chemists have been aiming for a long time to replicate nature's orchestration of these intricate ring-closing events.^[3] Since the groundbreaking work of Stork^[4] and Eschenmoser^[5-6] in 1955, rationalizing the stereoelectronic aspects of polyene cyclizations, there has been extensive research into developing reagent-based and catalytic methods for these transformations.^[7-9] Structural pre-organization of the flexible, linear polyene substrates, as explained in the biogenic isoprene rule^{[3-}

⁴), is the key to successfully controlling solution-phase conformations and, with that, steering the selectivity of such ring-closing events as enzymes can do. This, however, still constitutes a dream for organic chemists.

Currently, the only known pathways for terpene biosynthesis involve two-electron transfer and cation- π mechanisms. However, single-electron transfer (SET) reactions are also feasible with excellent diastereoselectivity, as demonstrated by Breslow et al. in the 1960s.^[10-11] The limited examples of radical terpene cyclizations to date have primarily depended on transition metals, such as Ti(III) or Ti(III)/Mn, which are often required in stoichiometric amounts.^[12] Seminal studies by Demuth^[13-20] have shown that radical polyene cyclizations can be initiated through photochemically induced electron transfer (PET, Figure 1a).^[21-22] In this process, the radical cation **3** generated from the photochemical oxidation of alkene **1** leads to a radical cyclization cascade and nucleophile addition (here MeOH) to the cation (Figure 1a). The transformation is concluded by reduction and protonation or by HAT from a suitable H-donor. Nonetheless, these transformations need high or often stoichiometric amounts of a photochemically active electron-acceptor system, such as *N*-methyl quinolinium salt (**2**)/biphenyl, UV light irradiation, and struggle with low yields and selectivities, together with a limited substrate scope.

In 2015, Zhang, Luo, and co-workers^[23] converted trien-ols **5** to the corresponding cyclohexyl products **7** (Figure 1b) by applying the xanthene dye eosin Y (**6**) as photocatalyst and illumination with green light. The reaction proceeded only in high yields and diastereoselectivities when 1,1,1,3,3,3-hexafluoro-isopropanol (HFIP) was used as the solvent. Fluorinated alcohols, such as HFIP and perfluoro-*tert*-butanol (PFTB), proved superior for ionic polyene cyclizations. They form dynamic, catalytically active F-alcohol-Lewis base clusters in situ that mimic the intrinsic properties of terpene cyclases, facilitating selective head-to-tail cyclizations of structurally different linear polyenes.^[24-27]

The mechanism of the eosin-catalyzed^[28] terpene cyclization has triggered a controversial debate among the scientific community.^[29-30] The authors claim that the reaction proceeds via a PET mechanism in analogy to the photoinduced cyclizations reported Demuth et al. (Figure 1a).^[13-22, 31-33] However, for the eosin Y-catalyzed transformations, no trapping of the elusive carbocation by nucleophilic addition or deprotonation, giving rise to the alkene products (not shown), was observable. In addition, the proposed direct photochemical oxidation of the alkene moiety by neither the singlet nor the triplet state of eosin Y (**6**) is possible when comparing the redox potential of EH_2^* (E_{red}^S ($^S\text{1EH}_2^*/\text{EH}_2^*$) = 1.23 V vs. SCE); E_{red}^T ($^T\text{1EH}_2^*/\text{EH}_2^*$) = 0.83 V vs. SCE)^[34] and that of trisubstituted alkenes (E_{ox} (sub^{•+}/sub) = ca. 2V,^[35] even when considering an increased redox potential in HFIP as proposed by Luo and Zhang (Figure 1b). An acid-mediated, ionic cyclization mechanism seems more consistent with the observation that the transformation leading to products **7** exhibiting the same stereo- and regioselectivity as in acid-mediated cyclizations.^[26, 36-38] In this context, photocatalytic oxidation of the phenol followed by protonation of the alkene moiety in **5** by the highly acidic phenol radical cation [$\text{pK}_a(\text{PhOH}^{\bullet+}) = -8.13$]^[39] was discussed by Nicewicz and co-workers.^[29] Another possible mechanistic scenario might be that photocatalyst **6** acts as a photoacid,^[40-41] facilitating protonation of the terminal alkene in **6** in the excited state, thus starting the proton-induced cyclization to **7**. Direct protonation of the alkene moiety in **5** by ground-state eosin Y (**6**, pK_a 2.0 and 3.8) or HFIP (pK_a 9.4)^[42-43] can be ruled out as neither **6** nor HFIP is acidic enough to protonate terminal alkenes.

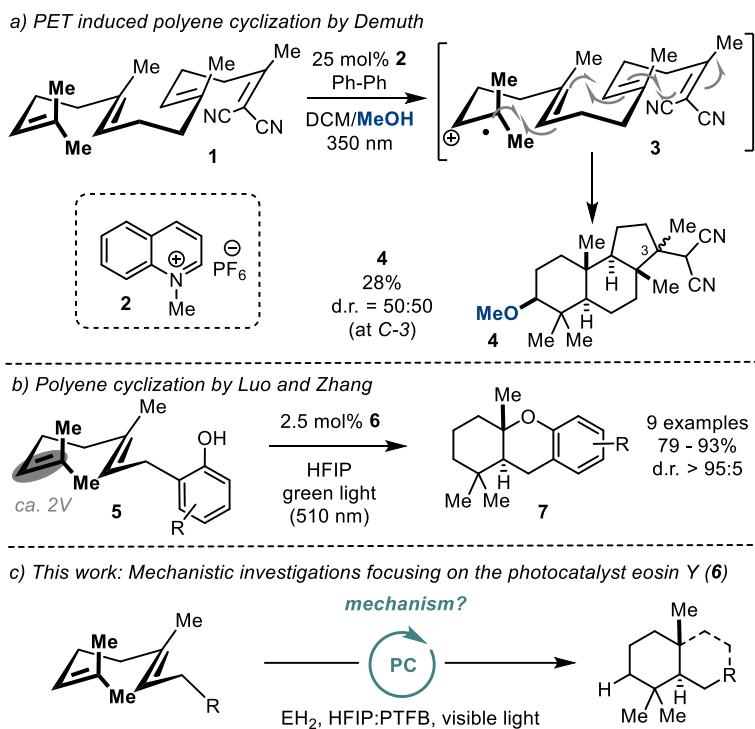
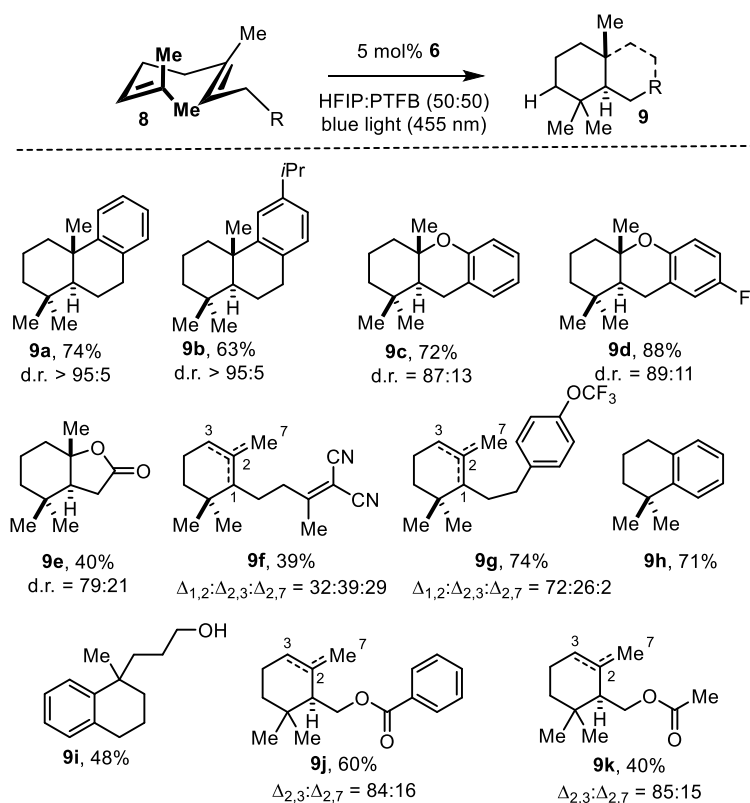


Figure 1. Photocatalytic Polyene Cyclizations.

Establishing photocatalytic radical terpene cyclizations as a versatile, mild, and selective alternative with orthogonal chemoselectivity to the extensively studied ionic transformations is highly desirable. Shedding light on the mechanistic scenario, particularly on the role of eosin Y (**6**) in this transformation, is necessary for rational and straightforward method development addressing a broad substrate and reaction scope in the future. Herein, we report on a new reaction mode of eosin Y (**6**) in photoredox reactions.

We started our investigations by re-evaluating the reaction conditions that led to the photocatalytic terpene formation in HFIP using eosin Y (**6**) as the catalyst. Thereby, it turned out that by changing from green to blue (455 nm) light, the reaction was more efficient, and even substrates devoid of electron-rich aromatic substituents, such as homogeryl benzene (**8a**), can be converted (Scheme 1 and SI). The corresponding cyclic product **9a** was obtained in 50% yield and perfect diastereoselectivity (d.r. > 95:5). Protonation-induced polyene cyclizations previously reported by the Gulder group^[25-27] showed a better outcome when PTFB was used as the solvent. In the photocatalytic transformation, however, the yield dropped significantly to 23%, but in a 50:50 mixture of HFIP:PTFB, the polyene cyclization was achieved in 74% with excellent diastereoselectivities (d.r. > 95:5). We exposed various acyclic substrates **8** to these conditions. The polyene cyclization proceeded smoothly in all cases. It chemoselectively gave (poly) cyclic products **9** with excellent diastereomeric ratios of up to >95:5 (Scheme 1), regardless of whether electron-donating or -withdrawing substituents are present. Although control experiments (no light, no photocatalyst) suggested that the polyene cyclization is a photocatalytic process, the chemo- and regioselectivity gave only products **9** that can also arise from an ionic protonation-induced ring-closing event.^[26] For example, the formation of cyclopentane derivatives and the conversion of substrates typical for radical cyclizations were not observed. The addressable substrate scope also rules out that phenol oxidation can solely trigger the reaction.



Scheme 1. Substrate Scope of the Eosin Y (**6**)-Catalyzed Polyene Cyclizations in HFIP:PTFB.

The xanthene dye **6** was crucial in all transformations. Other photocatalysts, especially those acting preferably via hydrogen atom transfer (HAT), did not yield **9a**). Exchanging the bromine substituents in **6** with other halogen atoms (F and Cl) or hydrogen also led to a significant decrease in yield. Employing the iodo analog erythrosine B as photocatalyst, the catalyst and product **9a** were significantly degraded, giving the terpene **9a** in poor 32% isolated yield. This behavior could be explained by the fact that the reaction only proceeds through the longer-lived triplet excited state of **6**. Additionally, no fluorescence quenching of **6** by adding homoggeranyl benzene (**8a**) was detectable, further corroborating this hypothesis.

In the next step, we looked closer at the photocatalyst eosin Y (**6**), particularly its properties in the microstructured F-alcohol environment. Eosin Y (**6**) can exist as several protolytic species, ranging from the cationic EH_3^+ to the dianionic E^{2-} , depending on the acidity or basicity of the medium. Each of these protonation states displays different chemical and photophysical properties.^{[44-45] [28]} The neutral EH_2 exists in a tautomeric equilibrium of the spirocyclic lactone EH_2 -lactone **6a** (closed form) and the carboxylic acid EH_2 **6b** (open form; Figure 2a).^[44, 46] The lactone **6a** is colorless, absorbing only UV light, while the carboxylic acid **6a** is colored orange (Figure 2b), absorbing near 480 nm (Figure 4b).^{[44] [47]}

In this study, we focused on the neutral EH_2 species **6** in a moderately acidic mixture of HFIP (pKa = 9.4) and PFTB (pKa = 5.4), confirmed qualitatively (Figure 2b) and quantitatively by the UV-vis absorption spectrum of **6** in HFIP, which shows only EH_2 , with no color change observed throughout the reaction (Figure 2c and 4b). NMR and UV-Vis titration experiments showed a strong interaction of the Lewis acid HFIP and the photocatalyst **6**. Adding HFIP to an eosin Y-dichloromethane (DCM) solution led to increased acidity of the mixture, accompanied by a bathochromic shift and an enhanced UV/Vis absorption between 350 nm and 550 nm (Figure 2c). This observation suggests that HFIP interacts with **6** most likely via hydrogen bonding, stabilizing the photoactive tautomer **6b**.^[48]

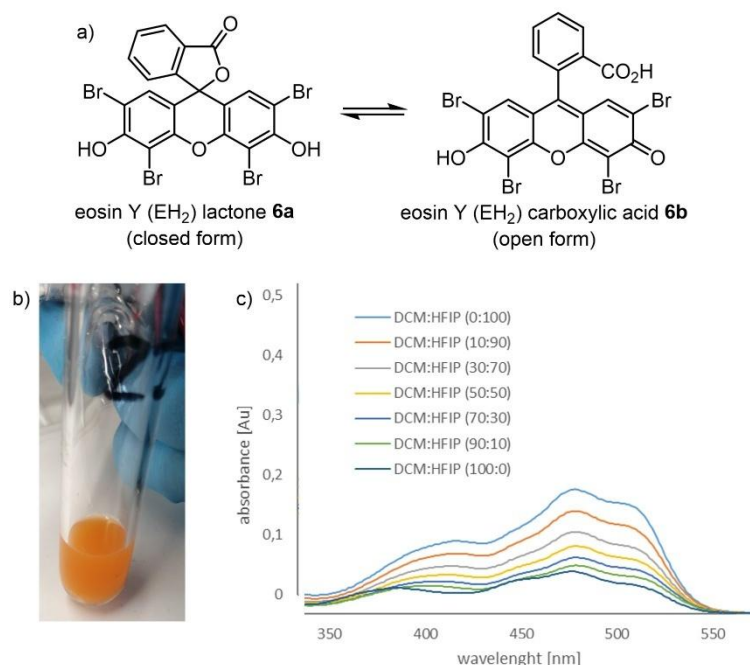


Figure 2. **a)** Equilibrium of the lactone **6a** (closed form) and the carboxylic acid **6b** (open form) for the neutral protolytic species EH₂. **b)** eosin Y (**6**) EH₂ in HFIP:PFTB (50:50). **c)** Increasing UV/Vis absorption due to stabilization of the open form **6b** of eosin Y upon addition of HFIP.

We conducted a computational study to understand why the open, carboxylic form **6b** is presumably more prevalent than the lactone form **6a**. Quantum mechanical calculations employing a continuum solvation model indicate that the closed form is energetically favored, with the open form being 26 kJ/mol higher in free energy. This holds despite **6b** exhibiting a larger solvation free energy, as predicted by the PCM model, due to its increased solvent-accessible surface area. This prediction suggests that the open form **6b** would not be prevalent under ambient conditions, contradicting experimental observations. However, it is well-established that HFIP can form powerful hydrogen bonds.^[25-27, 43, 49-51] Therefore, these computational results are unsurprising, considering the limitations of the solvent model used. Specifically, continuum models represent only average bulk solvent effects and neglect explicit interactions between eosin Y (**6**) and solvent molecules.^[52] This highlights the critical role of specific hydrogen bonding networks in determining the experimentally observed preference for the open form **6b**.

Hydrogen bonds between the HFIP molecules and **6** were analyzed over the 5-ns trajectory. Although the number of accessible hydrogen bond sites on eosin is identical in both the open and closed forms (see Fig. 3a), notable differences emerge. On average, the lactone **6a** has approximately one fewer hydrogen bond with HFIP than **6b**. This difference likely arises from the increased flexibility of the carboxyl group in **6b**, which enhances its steric accessibility. Concurrently, the HFIP–HFIP hydrogen bond network is slightly perturbed in the presence of the open eosin **6a**, as some HFIP molecules are redirected to interact with eosin instead (Figure 3b). This suggests that hydrogen bonding with **6** is energetically and entropically preferred over maintaining the HFIP network. Additionally, atom-wise radial distribution functions between **6** and HFIP (Figure 3c) further highlight the local structure of these interactions. In the open form, the O(2)–H group is readily accessible. It acts as a hydrogen bond donor, whereas in the closed form, the ester O(2) is sterically shielded and does not engage in close interactions. This structural difference favors a solvation pattern where HFIP molecules preferentially form hydrogen bonds with the O(2)–H of the open form **6b** (see Fig. 3a, right panel). Although the two neighboring HFIPs in this configuration do not fulfill the strict geometric criteria for hydrogen bonding,

their close proximity indicates the presence of interactions in the observed solvation pattern. These looser interactions help stabilize the disrupted HFIP network, further supporting the preferential formation of hydrogen bonds between the open eosin **6b** and HFIP molecules. This result was further corroborated by applying variations of eosin Y (**6**) with progressively removed O-H bonds in the form of eosin Y methyl ester, dimethyl eosin Y, and eosin Y sodium salts, which were ineffective in the terpene cyclization of **8a**, highlighting the importance of acidic protons for the cyclization event.

To quantify these interactions, we computed interaction energies at the quantum-chemical level using microsolvated clusters extracted from classical MD simulations. Figure 3d (left panel) shows that the electronic energy differences obtained with a continuum solvation model (PCM) cannot explain the observed preference for **6b**. In contrast, the explicitly computed interaction energies reveal an inverted trend, favoring the open form **6b**, likely due to its ability to form more hydrogen bonds. On a Boltzmann-weighted average, the open eosin Y (**6b**) has a stabilizing interaction energy of 103 kJ/mol higher than the spirocyclic form **6a**. This indicates that the solvation structure, particularly the formation of specific hydrogen bonds, plays a decisive role in stabilizing the open form **6b** of eosin Y over the closed one. This explains the experimentally observed trend.

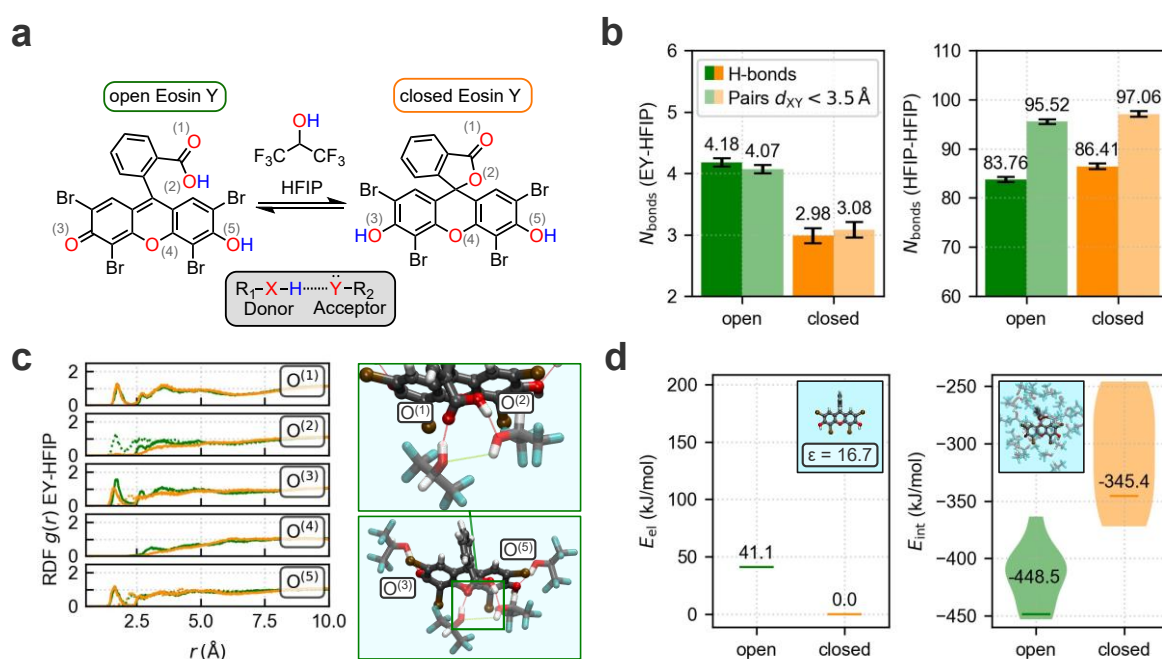


Figure 3. **a)** Scheme of intramolecular inversion of the Eosin Y with labeling of potential hydrogen bond donors and acceptors. **b)** Left panel: Average number of hydrogen bonds and number of unique donor–acceptor pairs, i.e., no triples, with a donor–acceptor distance d_{XY} below 3.5 Å between eosin Y (**6**, EH) and HFIP molecules. Right panel: Average number of hydrogen bonds and unique pairs within the HFIP network. All results are averaged over a 5 ns NVT simulation. The criterion for a hydrogen bond is a donor–acceptor distance d_{XY} below 3.5 Å and a maximum angle deviation of 30°. Error bars represent the standard deviation from block averaging over 10 blocks across the full trajectory. **c)** Left panel: pairwise radial distribution functions $g(r)$ between the labelled oxygen atoms (solid line) of the open (green, **6b**) and closed (orange, **6a**) eosin Y and the respective hydrogens (dotted line) if bound to an oxygen from MD simulations. The distance r is taken from the center of mass of the Eosin. Right Panel: characteristic hydrogen bonding pattern between $O^{(1)}$, $O^{(2)}$ and two HFIP molecules. Hydrogen bonds are displayed with a red dashed line, and the interaction between the HFIP molecules is shown with a green dashed line. **d)** Solvation and interaction energies from quantum-chemical calculations. Left panel: electronic energies of open **6b** and closed **6a** eosin Y using PCM. Right panel: interaction energies for 10 different clusters (grey) and the Boltzmann-weighted average for the open and closed Eosin Y. The Boltzmann weights are the total energies from the full MD snapshots. The clusters were extracted from classical MD simulations with a cutoff of 7 Å from the eosin to the OH group of the HFIP molecules to include all relevant hydrogen bonds. The exact definition of the interaction can be found in the SI.

Encouraged by the unprecedented behavior of eosin Y (**6**) in the fluorinated alcohol environment, we further investigated the photophysical and photochemical properties of EH₂ (**6**) in a solvent mixture of HFIP/PFTB (50/50 v%) utilizing fluorescence and UV-vis absorption spectroscopy. When excited with an appropriate light source, EH₂ (**6**) exhibits a weak orange fluorescence peaking at 550 nm (see Figure 4d). Using an integration sphere, the fluorescence quantum yield was determined to be $\Phi_{fl} = 1\%$ (equivalent to a rate constant of $k_{fl} = 1 \cdot 10^8 \text{ s}^{-1}$). In the fluorinated alcohol mixture, we determined the fluorescence lifetime to be $\tau_{fl} = 0.1 \text{ ns}$. This is noticeably shorter than the fluorescence lifetime $\tau_{fl} = 1.1 \text{ ns}$, 1.4 ns we found in toluene and dichloromethane, respectively. Since the lifetime of the excited singlet S₁ state is in the sub-ns regime, we next carried out transient absorption (TA) spectroscopy with sub-ps time resolution based on ultrafast pump-probe spectroscopy (Figure 4a). This again confirmed the lifetime of the S₁ state to be $\tau_{fl} = 0.1 \text{ ns}$. The S₁ state is characterized by an excited state absorption (ESA) at 360 nm, a ground state bleach (GSB) at 480 nm, and stimulated emission (SE) in the red spectral region (530-650 nm). The S₁ state then decays into a non-fluorescent excited state, which shows a characteristic broad positive absorption change at >537 nm. We assign this to triplet-triplet absorption and, therefore, the non-fluorescent state to the triplet T₁ (see Scheme 2, ISC). We estimate the intersystem crossing efficiency to be approximately $\Phi_{ISC} = 60\%$ (equivalent to a rate constant of $k_{ISC} = 6 \cdot 10^9 \text{ s}^{-1}$). The T₁ state is significantly longer-lived than the 6 ns time window of the sub-ps TA. Consequently, we extended the TA measurement window to the μs regime, now using streak camera-based detection (see Figure 4b). The T₁ state decays in tens of microseconds and is very efficiently quenched by atmospheric oxygen, which is typical for triplet states (see Figure 4e).^[53]

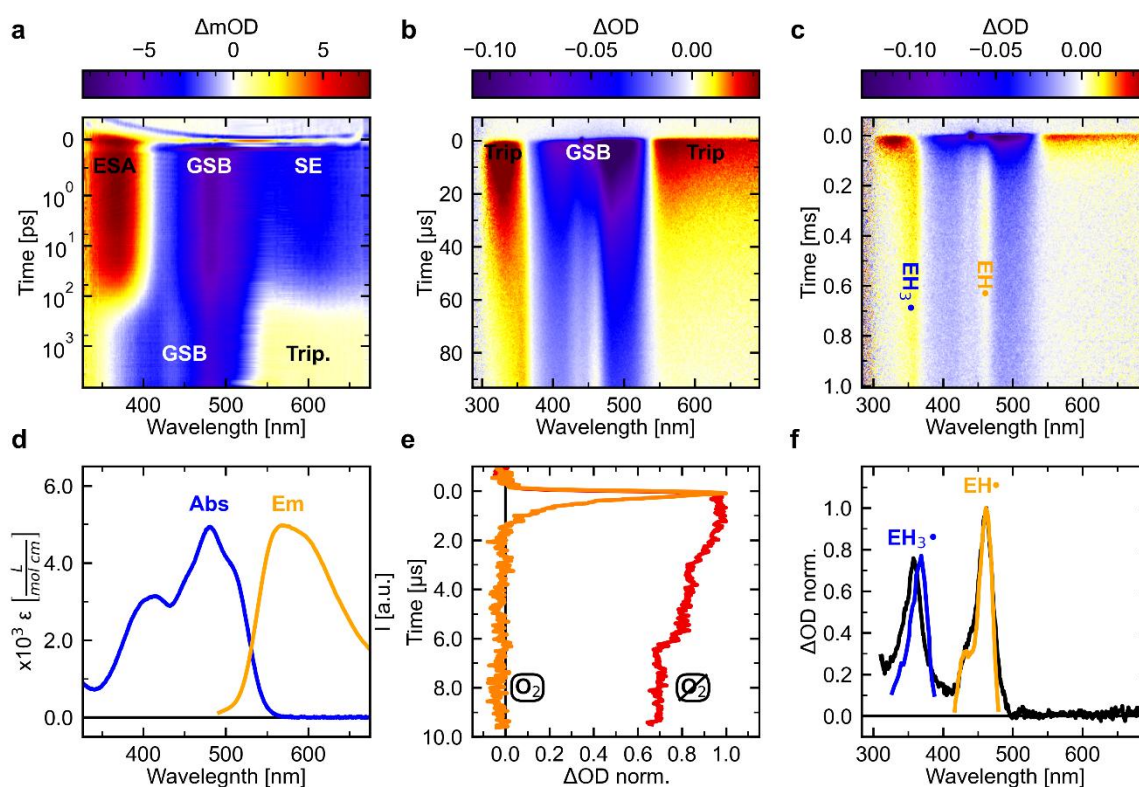


Figure 4. **a)** sub-ps TA spectra of EH₂ **6** in HFIP/PFTB (excitation wavelength 530 nm). **b)** μs -TA of EH₂ **6** in HFIP/PFTB (excitation wavelength 440 nm). **c)** ms-TA of EH₂ **6** in HFIP/PFTB (excitation wavelength 440 nm). **d)** Absorption coefficient (blue line) and emission spectrum (orange line, excitation wavelength 481 nm) of EH₂ **6** in HFIP/PFTB. **e)** Triplet decay of EH₂ **6** monitored by the triplet-triplet absorption above 537 nm without (red line) and with (orange line) atmospheric oxygen present. **f)** Absorption peaks of EH₃[•] and EH[•] extracted from the ms-

TA measurement of EH_2 **6** in HFIP/PFTB (black line) compared to the absorption spectrum of EH_3^\bullet in tetrahydrofuran (THF).^[54] (blue line) and absorption spectrum of EH^\bullet produced by HAT from EH_2 to tert-butyl alkoxy radical (orange line). ESA: excited state absorption, GSB: ground state bleach, SE: stimulated emission, Trip.: triplet-triplet absorption.

While the spectral features of the T_1 -state decay, two new positive bands at 360 nm and 460 nm appear, which rise at the same rate. These features persist for over 1 ms but eventually decay (see Figure c). The absorption at 360 nm was assigned to the EH_3^\bullet radical (see Figure 4f), which is formed when **6** abstracts a hydrogen atom from another molecule by Fan *et al.*^[54] Since there are no other molecules present except the fluorinated alcohol solvent molecules, which are not prone to undergo HAT, we reasoned that the absorption at 460 nm must correspond to the EH^\bullet radical (see Figure 4f), which is formed when a hydrogen atom is abstracted from EH_2 (see Scheme 2). The exact same absorption at 460 nm was observed when $t\text{Bu}_2\text{O}_2$ was added to **6** (see Figure 4f and SI). Here, photocleavage of the peroxide gave the corresponding hydrogen atom, abstracting the alkoxy radical that can undergo HAT with EH_2 and produce EH^\bullet .^[55-57] The absorptions corresponding to the two radicals EH_3^\bullet and EH^\bullet decay with the same rate, forming EH_2 again in the S_0 ground state by recombination of EH_3^\bullet and EH^\bullet (see Scheme 2). In toluene, the lifetime of EH^\bullet was significantly shorter than that of EH_3^\bullet , as EH^\bullet can abstract a hydrogen atom from the benzylic position of toluene, thus rebuilding EH_2 . When EH^\bullet was entirely consumed, the EH_3^\bullet decay plateaued, lacking a recombination partner. Changing the solvent to α,α,α -trifluorotoluene, formation of EH_2 was again possible only by recombining the two radical species, which resulted in both radicals EH_3^\bullet and EH^\bullet decaying at the same rate.

EH_3^\bullet and EH^\bullet formation can occur by HAT of two eosin Y (**6**) molecules in the T_1 state or by one EH_2 **6** in the T_1 and one in the S_0 ground state. Therefore, we conducted the TA experiments using different pump powers and different concentrations of EH_2 . Reducing the pump power from 6 mJ to 1 mJ led to an approximate halving of the transient concentration of T_1 . The T_1 decay rate remained unchanged, as observed by the decay of the triplet-triplet absorption above 537 nm (see Figure 5a). With increasing concentration of EH_2 **6**, the T_1 decay accelerated (see Figure 5b), showing that the HAT occurs between a T_1 EH_2 and a S_0 EH_2 (see Scheme 2).

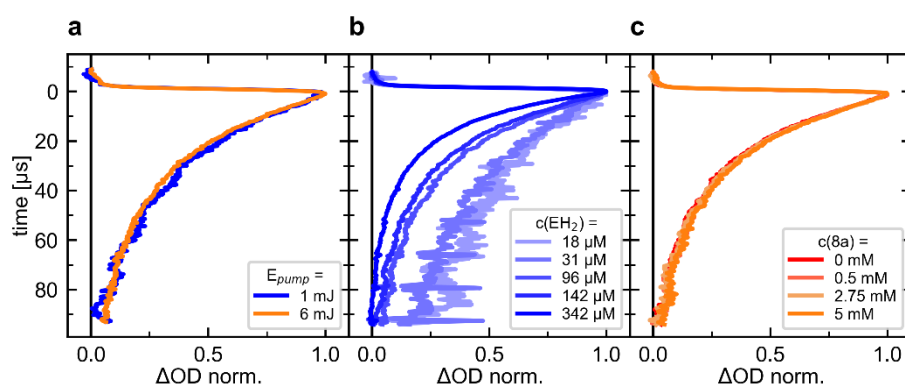


Figure 5. Triplet decay of EH_2 **6**, monitored by the triplet-triplet absorption above 537 nm, was recorded a) with 1 mJ and 6 mJ pump power, resulting in different transient concentrations of the T_1 state, b) at different ground-state concentrations of EH_2 **6**, and c) with different concentrations of **8a**.

Finally, we added different concentrations of substrate **8a** to the EH_2 **6** solution (see Figure 5c and 6). In the experiments only employing EH_2 **6**, the eosin Y solution was reasonably stable under irradiation

by ambient light or the used pump sources. However, when adding **8a** to the solution, **6** decomposed when exposed to light. Increasing the concentration of the added **8a** also increased the decomposition. No homogeranyl benzene (**8a**) interaction with the T_1 state of **6** was observed, as the decay rate of the T_1 state of **6** remained unchanged (see Figure 5c). The decay rates of the absorptions associated with the radicals EH_3^\bullet (360 nm) and EH^\bullet (460 nm), however, were affected (see Figure 6). Similar to the experiment conducted in toluene, the consumption of EH^\bullet sped up by increasing amounts of **8a** added (Figure 6d). In contrast, the decay rate of EH_3^\bullet slowed down upon adding **8a** (Figure 6c) because of the competing reaction with **8a**. This observation concludes that the in-situ formed EH^\bullet is the reactive species starting the polyene cyclizations by reacting with alkenes **8**.

When observing the signal intensity at 360 nm, which corresponds to the absorption of EH_3^\bullet , it is noted that at 3.5 to 4 ms, the signal converges to about 40% of its initial intensity as the concentration of compound **1** increases (see the inset in Figure 6c). If EH_3^\bullet were solely consumed through recombination with EH^\bullet , we would expect the intensity to converge at 100% for high concentrations of **8a**. Therefore, we propose that a second reaction, possibly involving an intermediate in the cyclization of **8a**, may also take place, consuming EH_3^\bullet . Numerical simulations of this kinetic model, using various concentrations of **8a**, confirmed that the transient concentrations of EH_3^\bullet converge at longer time delays.

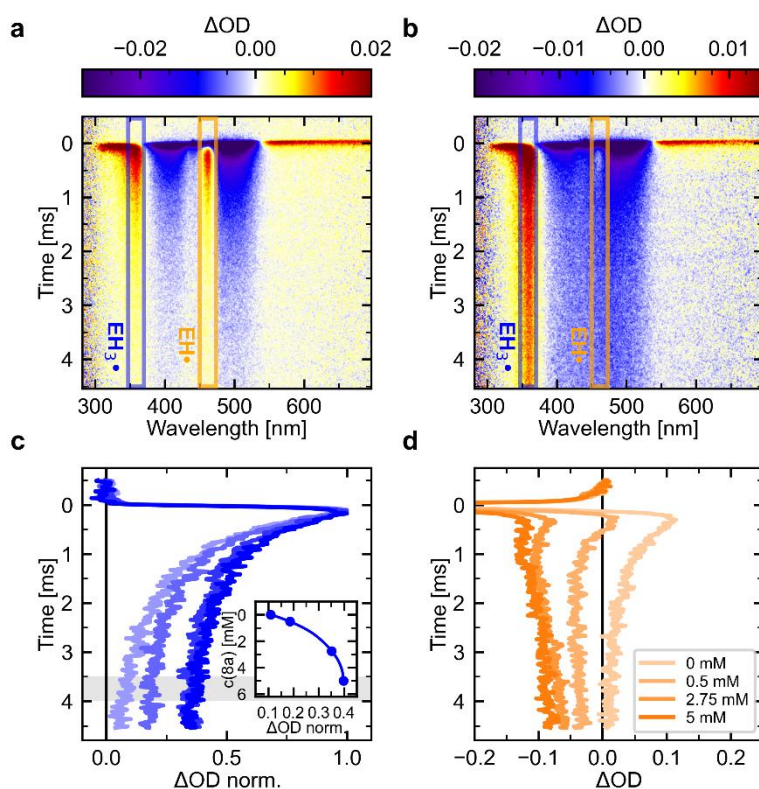
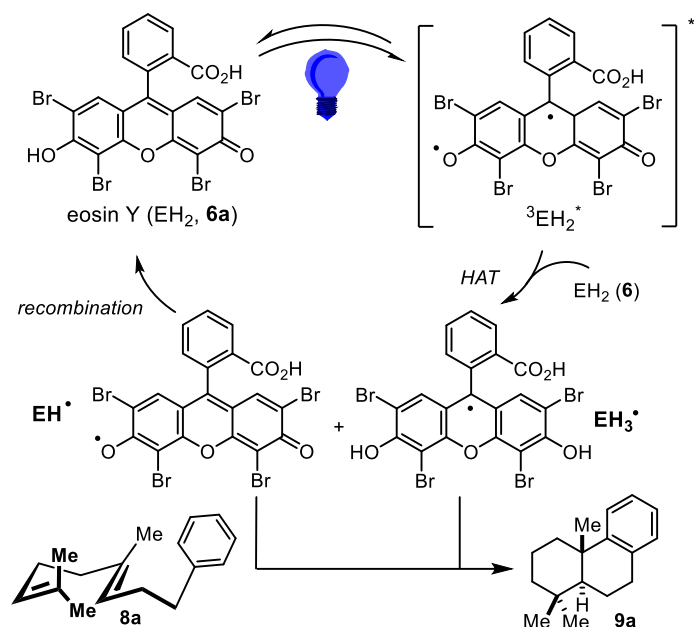


Figure 6. ms-TA of EH_2 **6** in HFIP/PFTB (excitation wavelength 440 nm): **a**) without **8a** and **b**) with 5 mM **8a** present. **c**) Averaged and normalized transients of the signal at 347-370 nm associated with the absorption of EH_3^\bullet with different concentrations **8a** (from light to dark blue: 0, 0.5, 2.75, 5 mM) present. Inset: Average signal at 3.5 - 4 ps (blue dots) and quadratic spline (blue line). **d**) Averaged and normalized signal transient at 450-473 nm associated with the absorption of EH_3^\bullet with different concentrations of **8a** present.

This study presents a comprehensive investigation into the photocatalytic behavior of eosin Y (**6**) in fluorinated alcohol environments. By employing a 1:1 mixture of HFIP and PFTB, we demonstrate that the neutral form of eosin Y (**6**, EH_2) undergoes efficient intersystem crossing to its triplet state, which subsequently engages in hydrogen atom transfer (HAT) with ground-state EH_2 (Scheme 2). This process

generates two distinct radical species, EH^\bullet and EH_3^\bullet , that either recombine or productively react with polyene substrates **8**. In this reaction sequence, the radical EH^\bullet was identified as the key reactive species starting the cyclization of terpene substrates **8**, while EH_3^\bullet may participate in subsequent steps. The fluorinated alcohol network played a crucial role in this transformation, as no reaction can be witnessed in other solvents. Mechanistic studies, including spectroscopy and quantum chemical calculations, revealed a distinct hydrogen-bonding network of the photocatalyst **6** and HFIP/PFTB stabilizing the visible light photoactive, open carboxylic acid form of EH_2 (**6b**), despite being thermodynamically less favored in the absence of explicit solvation.



Scheme 2. Eosin Y (**6**) disproportionation mechanism occurs after the excitation of EH_2 in HFIP/PFTB, which is the key step in initiating polyene cyclizations.

In conclusion, our findings establish a novel mechanistic paradigm for eosin Y-catalyzed photochemical transformations, wherein the photocatalyst undergoes self-disproportionation via HAT to generate two reactive radical species. This dual-radical generation from a single photocatalyst molecule introduces a new dimension to photoredox catalysis. The unique solvation effects of fluorinated alcohols stabilize the photoactive form of eosin Y and facilitate the desired reactivity through hydrogen bonding networks.

This work clarifies the long-debated mechanism of eosin Y-mediated cyclizations and opens avenues for the rational design of new photocatalytic systems leveraging similar disproportionation strategies. Future efforts will focus on expanding the substrate and reaction scope to be addressed by this reaction mechanism, aiming to expand the synthetic toolbox to new and sustainable transformations.

Conflicts of interest

There are no conflicts to declare.

Acknowledgements

This work was funded by the Deutsche Forschungsgemeinschaft (DFG, German Research Foundation) within the TRR 325 – 444632635.

References

- [1] D. W. Christianson, "Structural and Chemical Biology of Terpenoid Cyclases" *Chem. Rev.* **2017**, *117*, 11570-11648.
- [2] D. W. Christianson, "Structural Biology and Chemistry of the Terpenoid Cyclases" *Chem. Rev.* **2006**, *106*, 3412-3442.
- [3] R. A. Yoder, J. N. Johnston, "A Case Study in Biomimetic Total Synthesis: Polyolefin Carbocyclizations to Terpenes and Steroids" *Chem. Rev.* **2005**, *105*, 4730-4756.
- [4] G. Stork, A. W. Burgstahler, "The stereochemistry of polyene cyclization" *J. Am. Chem. Soc.* **1955**, *77*, 5068-5077.
- [5] A. Eschenmoser, D. Arigoni, "Revisited after 50 years: The 'stereochemical interpretation of the biogenetic isoprene rule for the triterpenes'" *Helvetica Chimica Acta* **2005**, *88*, 3011-3050.
- [6] A. Eschenmoser, L. Ruzicka, O. Jeger, D. Arigoni, "Triterpenes. CXC. A stereochemical interpretation of the biogenetic isoprene rule of the triterpenes" *Helvetica Chimica Acta* **1955**, *38*, 1890-1904.
- [7] A. G. M. Barrett, T.-K. Ma, T. Mies, "Recent Developments in Polyene Cyclizations and Their Applications in Natural Product Synthesis" *Synthesis* **2019**, *51*, 67-82.
- [8] C. N. Ungarean, E. H. Southgate, D. Sarlah, "Enantioselective polyene cyclizations" *Org. Biomol. Chem.* **2016**, *14*, 5454-5467.
- [9] M. A. Schafroth, D. Sarlah, S. Krautwald, E. M. Carreira, "Iridium-Catalyzed Enantioselective Polyene Cyclization" *J. Am. Chem. Soc.* **2012**, *134*, 20276-20278.
- [10] R. Breslow, J. T. Groves, S. S. Olin, "Novel oxidative terpene cyclization" *Tetrahedron Lett.* **1966**, 4717-4719.
- [11] R. Breslow, E. Barrett, E. Mohacsi, "Free radical additions to squalene" *Tetrahedron Lett.* **1962**, 1207-1211.
- [12] J. Justicia, L. Alvarez de Cienfuegos, A. G. Campana, D. Miguel, V. Jakoby, A. Gansaeuer, J. M. Cuerva, "Bioinspired terpene synthesis: a radical approach" *Chem. Soc. Rev.* **2011**, *40*, 3525-3537.
- [13] V. Rosales, J. Zambrano, M. Demuth, "Straightforward synthesis of aromatic polycyclic terpenoids through biomimetic cascade cyclizations triggered by photochemical electron transfer" *Eur. J. Org. Chem.* **2004**, 1798-1802.
- [14] Mustafa E. Ozser, H. Icil, Y. Makhynya, M. Demuth, "Electron-Transfer-Initiated Cascade Cyclizations of Terpenoid Polyalkenes in a Low-Polarity Solvent: One-Step Synthesis of Mono- and Polycyclic Terpenoids with Various Functionalities" *Eur. J. Org. Chem.* **2004**, *2004*, 3686-3692.
- [15] F. Goeller, C. Heinemann, M. Demuth, "Investigations of cascade cyclizations of terpenoid polyalkenes via radical cations. A biomimetic-type synthesis of (\pm)-3-hydroxy-spongian-16-one" *Synthesis* **2001**, 1114-1116.
- [16] X. Xing, M. Demuth, "Application of photoinduced biomimetic cascade cyclizations of terpenoid polyalkenes for the synthesis of (\pm)-stypoldione" *Eur. J. Org. Chem.* **2001**, 537-544.
- [17] C. Heinemann, M. Demuth, "Short Biomimetic Synthesis of a Steroid by Photoinduced Electron Transfer and Remote Asymmetric Induction" *J. Am. Chem. Soc.* **1999**, *121*, 4894-4895.
- [18] X. Xing, M. Demuth, "An efficient formal total synthesis of (\pm)-stypoldione via photochemically triggered biomimetic cyclizations of terpenoid polyalkenes" *Synlett* **1999**, 987-990.

- [19] C. Heinemann, M. Demuth, "Biomimetic Cascade Cyclizations of Terpenoid Polyalkenes via Photoinduced Electron Transfer. Long-Distance Asymmetric Induction by a Chiral Auxiliary" *J. Am. Chem. Soc.* **1997**, *119*, 1129-1130.
- [20] U. Hoffmann, Y. Gao, B. Pandey, S. Klinge, K. D. Warzecha, C. Krueger, H. D. Roth, M. Demuth, "Light-induced polyene cyclizations via radical cations in micellar medium" *J. Am. Chem. Soc.* **1993**, *115*, 10358-10359.
- [21] K.-D. Warzecha, H. Gorner, M. Demuth, "Photoinduced electron transfer from isoprenoid polyalkene acetates to dicyanoarenes" *J. Chem. Soc., Faraday Trans.* **1998**, *94*, 1701-1706.
- [22] H. Gorner, K.-D. Warzecha, M. Demuth, "Cyclization of terpenoid dicyanitrile polyalkenes upon photoinduced electron transfer to 1,4-dicyano-2,3,5,6-tetramethylbenzene and other cyanoarenes" *J. Phys. Chem. A* **1997**, *101*, 9964-9973.
- [23] Z. Yang, H. Li, L. Zhang, M.-T. Zhang, J.-P. Cheng, S. Luo, "Organic Photocatalytic Cyclization of Polyenes: A Visible-Light-Mediated Radical Cascade Approach" *Chem. Eur. J.* **2015**, *21*, 14723-14727.
- [24] N. Luo, M. Turberg, M. Leutzsch, B. Mitschke, S. Brunen, V. N. Wakchaure, N. Nöthling, M. Schelwies, R. Pelzer, B. List, "The catalytic asymmetric polyene cyclization of homofarnesol to ambrox" *Nature* **2024**, *632*, 795-801.
- [25] J. Binder, A. Biswas, T. Gulder, "Biomimetic chlorine-induced polyene cyclizations harnessing hypervalent chloriodane–HFIP assemblies" *Chem. Sci.* **2023**, *14*, 3907-3912.
- [26] A. M. Arnold, P. Dullinger, A. Biswas, C. Jandl, D. Horinek, T. Gulder, "Enzyme-like polyene cyclizations catalyzed by dynamic, self-assembled, supramolecular fluoro alcohol-amine clusters" *Nat. Commun.* **2023**, *14*, 813.
- [27] A. M. Arnold, A. Poethig, M. Drees, T. Gulder, "NXS, Morpholine, and HFIP: The Ideal Combination for Biomimetic Haliranium-Induced Polyene Cyclizations" *J. Am. Chem. Soc.* **2018**, *140*, 4344-4353.
- [28] M. Majek, F. Filace, A. J. v. Wangelin, "On the mechanism of photocatalytic reactions with eosin Y" *Beilstein Journal of Organic Chemistry* **2014**, *10*, 981-989.
- [29] N. A. Romero, D. A. Nicewicz, "Organic Photoredox Catalysis" *Chem. Rev.* **2016**, *116*, 10075-10166.
- [30] S. Bhattarai, A. Kafle, S. T. Handy, "Catalyst-free light-mediated polyene cyclization" *Tetrahedron* **2024**, *156*, 133910.
- [31] K.-D. Warzecha, X. Xing, M. Demuth, "Cyclization of terpenoid polyalkenes via photoinduced electron transfer - versatile single-step syntheses of mono- and polycycles" *Pure Appl. Chem.* **1997**, *69*, 109-112.
- [32] K.-D. Warzecha, M. Demuth, H. Gorner, "Photocyclization of terpenoid polyalkenes upon electron transfer to a triphenylpyrylium salt. A time-resolved study" *J. Chem. Soc., Faraday Trans.* **1997**, *93*, 1523-1530.
- [33] K.-D. Warzecha, X. Xing, M. Demuth, R. Goddard, M. Kessler, C. Krueger, "Cascade cyclizations of terpenoid polyalkenes triggered by photoelectron transfer. Biomimetics with photons" *Helvetica Chimica Acta* **1995**, *78*, 2065-2076.
- [34] T. Shen, Z.-G. Zhao, Q. Yu, H.-J. Xu, "Photosensitized reduction of benzil by heteroatom-containing anthracene dyes" *Journal of Photochemistry and Photobiology A: Chemistry* **1989**, *47*, 203-212.
- [35] H. G. Roth, N. A. Romero, D. A. Nicewicz, "Experimental and Calculated Electrochemical Potentials of Common Organic Molecules for Applications to Single-Electron Redox Chemistry" *Synlett* **2016**, *27*, 714-723.
- [36] A. Sakakura, M. Sakuma, K. Ishihara, "Chiral Lewis Base-Assisted Brønsted Acid (LBBA)-Catalyzed Enantioselective Cyclization of 2-Geranylphenols" *Org. Lett.* **2011**, *13*, 3130-3133.
- [37] K. Ishihara, S. Nakamura, H. Yamamoto, "The First Enantioselective Biomimetic Cyclization of Polyprenoids" *J. Am. Chem. Soc.* **1999**, *121*, 4906-4907.
- [38] R. L. Snowden, S. Linder, "Internal Nucleophilic Termination in Acid-Mediated Polyene Cyclizations Part 4" *Helv. Chim. Acta* **2005**, *88*, 3055-3068.

- [39] F. G. Bordwell, J. P. Cheng, "Radical-cation acidities in solution and in the gas phase" *J. Am. Chem. Soc.* **1989**, *111*, 1792-1795.
- [40] D.-M. Yan, J.-R. Chen, W.-J. Xiao, "New Roles for Photoexcited Eosin Y in Photochemical Reactions" *Angew. Chem. Int. Ed* **2019**, *58*, 378-380.
- [41] J. Tripathi, H. Gupta, A. Sharma, "Photoacid-Catalyzed Esterification of Carboxylic Acids Using Eosin Y" *Organic Letters* **2025**, *27*, 1018-1023.
- [42] I. Colomer, A. E. R. Chamberlain, M. B. Haughey, T. J. Donohoe, "Hexafluoroisopropanol as a highly versatile solvent" *Nat. Rev. Chem.* **2017**, *1*, 0088.
- [43] H. F. Motiwala, A. M. Armaly, J. G. Cacioppo, T. C. Coombs, K. R. K. Koehn, V. M. Norwood, J. Aubé, "HFIP in Organic Synthesis" *Chem. Rev.* **2022**, *122*, 12544–12747.
- [44] N. O. McHedlov-Petrosyan, V. I. Kukhtik, V. D. Bezugliy, "Dissociation, tautomerism and electroreduction of xanthene and sulfonephthalein dyes in N,N-dimethylformamide and other solvents" *J. Phys. Org. Chem.* **2003**, *16*, 380-397.
- [45] N. O. Mchedlov-Petrosyan, "Ionization and Tautomerism of Hydroxyxanthenes and Some Other Dyes in Ethanol" *Russian Journal of General Chemistry* **2003**, *73*, 267-274.
- [46] N. O. Mchedlov-Petrosyan, V. I. Kukhtik, V. I. Alekseeva, "Ionization and Tautomerism of Fluorescein, Rhodamine B, N,N-Diethylrhodol and Related Dyes in Mixed and Nonaqueous Solvents" *Dyes and Pigments* **1994**, *24*, 11-35.
- [47] V. R. Batistela, D. S. Pellosi, F. D. De Souza, W. F. Da Costa, S. M. De Oliveira Santin, V. R. De Souza, W. Caetano, H. P. M. De Oliveira, I. S. Scarminio, N. Hioka, "pKa determinations of xanthene derivatives in aqueous solutions by multivariate analysis applied to UV–Vis spectrophotometric data" *Spectrochimica Acta Part A: Molecular and Biomolecular Spectroscopy* **2011**, *79*, 889-897.
- [48] E. A. Slyusareva, M. A. Gerasimova, "pH-Dependence of the Absorption and Fluorescent Properties of Fluorone Dyes in Aqueous Solutions" *Russ. Phys. J.* **2014**, *56*, 1370.
- [49] Y. Ni, J. Lebelt, M. Barp, F. Kreuter, J. Jin, H. Buttkeus, M. Kretschmar, R. Tonner-Zech, K. R. Asmis, T. Gulder, "Hexafluorophosphate-Triggered Hydrogen Isotope Exchange (HIE) in Fluorinated Environments: A Platform for the Deuteration of Aromatic Compounds via Strong Bond Activation" *Angew. Chem. Int. Ed.* **2025**, *64*, e202417889.
- [50] F. Caporaletti, L. Gunkel, M. Á. Fernández-Ibáñez, J. Hunger, S. Woutersen, "Fast Collective Hydrogen-Bond Dynamics in Hexafluoroisopropanol Related to its Chemical Activity" *Angew. Chem. Int. Ed.* **2024**, *63*, e202416091.
- [51] I. Colomer, C. Batchelor-McAuley, B. Odell, T. J. Donohoe, R. G. Compton, "Hydrogen Bonding to Hexafluoroisopropanol Controls the Oxidative Strength of Hypervalent Iodine Reagents" *J. Am. Chem. Soc.* **2016**, *138*, 8855-8861.
- [52] J. M. Herbert, "Dielectric continuum methods for quantum chemistry" *WIREs Comp. Mol. Sci.* **2021**, *11*, e1519.
- [53] K. Kawaoka, A. U. Khan, D. R. Kearns, "Role of Singlet Excited States of Molecular Oxygen in the Quenching of Organic Triplet States" *The Journal of Chemical Physics* **1967**, *46*, 1842-1853.
- [54] X.-Z. Fan, J.-W. Rong, H.-L. Wu, Q. Zhou, H.-P. Deng, J. D. Tan, C.-W. Xue, L.-Z. Wu, H.-R. Tao, J. Wu, "Eosin Y as a Direct Hydrogen-Atom Transfer Photocatalyst for the Functionalization of C–H Bonds" *Angew. Chem. Int. Ed.* **2018**, *57*, 8514-8518.
- [55] C. Walling, A. Padwa, "Positive Halogen Compounds. VI. Effects of Structure and Medium on the β -Scission of Alkoxy Radicals" *J. Am. Chem. Soc.* **1963**, *85*, 1593-1597.
- [56] J. R. Shelton, C. W. Uzelmeier, "Reactions of alkenes with di-tert-butyl peroxide and tert-butyl peroxyphthalate" *J. Org. Chem.* **1970**, *35*, 1576-1581.
- [57] R. Oyama, M. Abe, "Reactivity and Product Analysis of a Pair of Cumyloxyl and tert-Butoxyl Radicals Generated in Photolysis of tert-Butyl Cumyl Peroxide" *J. Org. Chem.* **2020**, *85*, 8627-8638.